Soft Matter

Dimerization and Structure Formation of Colloids via Capillarity at Curved Fluid Interfaces

Journal:	*Soft Matter*
Manuscript ID	SM-ART-03-2020-000557.R1
Article Type:	Paper
Date Submitted by the Author:	28-May-2020
Complete List of Authors:	Read, Alismari; University of Pennsylvania, Chemical Engineering Kandy, Sreeja; University of Pennsylvania, Bioengineering Radhakrishnan, Ravi; University of Pennsylvania, Bioengineering; University of Pennsylvania Stebe, Kathleen; University of Pennsylvania, Liu, Iris; University of Pennsylvania,

Soft Matter

ARTICLE TYPE

Cite this: DOI: 00.0000/xxxxxxxxxx

Dimerization and Structure Formation of Colloids via Capillarity at Curved Fluid Interfaces

Alismari Read, Sreeja Kutti Kandy, Iris B. Liu, Ravi Radhakrishan and Kathleen J. Stebe[a]

Received Date
Accepted Date

DOI: 00.0000/xxxxxxxxxx

Capillary interactions are ubiquitous between colloids trapped at fluid interfaces. Generally, colloids in fluid interfaces have pinned, undulated contact lines that distort the interface around them. To minimize the area, and therefore the energy of these distortions, colloids interact and assemble in a manner that depends on the shape of the host interface. On curved interfaces, capillary interactions direct isolated colloid motion along deviatoric curvature gradients. This directed motion relies on the leading order, long-ranged quadrupolar distortions made by the colloids' undulated pinned contact lines. Here we study pair interactions and dimer formation of colloids on non-uniformly curved fluid interfaces. Pair interaction energies are inferred to be order of $10^4 k_B T$, and interacting forces are of order 10^{-1} pN for 10 micron particles adsorbed on interfaces formed around a 250 micron micropost. We compare experiments to analysis for the pair interaction energy, and identify criteria for dimers to form. We also study the formation of trapped structures by multiple particles to discern the influence of the underlying interface shape and the contact line undulations. By comparison to Monte Carlo simulations with potentials of interactions based on analysis, we find that higher order terms in the distortion fields generated by the particles play a major role in the structure formation on the curved interface. These interactions are determined by the particle's contact line and the host interface shape, and can be used to assemble particles independent of their material properties.

1 Introduction

The macroscopic behavior of complex materials depends on the organization of their constituents, including microscopic particles or colloids within them. Engineered soft materials with colloidal components are widely exploited in diverse fields including pharmaceuticals[1] and personal care,[2] and are important elements in emerging advanced metamaterials.[3] Classically, in suspension, colloid properties are used to influence colloid organization by tuning suspension properties to guide colloids to self assemble into structures that include crystals, disordered gels, and glasses.[4] To access other structures, externals fields, often electromagnetic in origin, are used to guide assembly.[5–7]

Colloids can also accumulate and organize at or near the interface between immiscible fluids. When adsorbed on fluid interfaces, colloids form a variety of structures, including closed packed structures,[8] ordered crystalline structures determined by the balance of capillary and electrostatic interactions,[9] and disordered structures influenced by near field capillary attraction.[10] Curvature is known to alter colloid organization fundamentally. For example, repulsive colloids adjacent to curved fluid interfaces and other curved boundaries reveal required defects in packings as a function of Gaussian curvature.[11,12] While the importance of curvature is well appreciated, its role in guiding structure formation by many colloids adsorbed on fluid interfaces has not been well-studied. In this research, we focus on the behavior of microparticles trapped on curved interfaces, and on the understanding of how curvature gradients and curvature capillary interactions influence particle organization. Hereafter, we refer to individual microparticles as colloids.

When particles adsorb on fluid interfaces, the highly anisotropic interfacial environment dramatically alters classical colloid interactions, and introduces capillary interactions. These latter interactions can be dominant and dictate colloidal organization.[13–16] A colloidal particle attached to a fluid interface decreases the energy of the system by replacing an area or patch of the interface with the colloid itself. Once attached, the colloid does not desorb spontaneously, as the reduction in energy upon attachment is typically many orders of magnitude larger than thermal energies.[9] Typically, colloids at interfaces do not attain equilibrium wetting configurations, but rather assume non-equilibrium trapped states that result in an undulated three phase contact line where the interface intersects the particle (inset of Fig.1(a)).[17] As a result, around each colloid, the interfacial shape is distorted; this distortion field decays with distance

---

[a] Chemical and Biomolecular Engineering, University of Pennsylvania, Philadelphia, PA, 19104, USA. E-mail: kstebe@seas.upenn.edu

† Electronic Supplementary Information (ESI) available. See DOI: 10.1039/cXsm00000x/

from the particle. Contact line pinning occurs at sites of particle chemical heterogeneity or surface roughness.[11,14] Particle shape anisotropy[18,19] also generates undulated contact lines with associated interface distortion that can be far larger than that typically observed for pinned contact lines on spherical particles. Finally, particle weight[20] or other body forces on a particle can distort the interface. Often, for colloids that are sufficiently small, the particle weight can be neglected. In this case, the distortion fields are not determined by the colloid material properties or suspension chemistry, but rather by the random pinning of the particle contact line and the shape of the surrounding interface. For all colloids with negligible weight, the leading order distortion generated by pinned contact lines in the surrounding interface has quadrupolar symmetries.

When a pair of particles trapped at a fluid interface are close enough for their distortion fields to overlap, the area of the interface changes. Capillary interactions are defined as the product of this change in interface area and the surface tension. Capillary interactions drive colloidal attraction in preferred orientations that minimize the interfacial area.[14,15] A dilute, random distribution of particles on a planar interface have no preferred site for assembly. Rather, capillary interactions occur between proximate particles with overlapping distortion fields. Microparticles attract to form dimers or other aggregates that are typically trapped owing to high strength of capillary attraction between them. However, for a non-uniformly curved host interface, the curvature generates a capillary energy field that directs particles along curvature gradients to specific locations and may guide them into well-defined structures. This phenomenon relies on the dependence of the particle's distortion field on the host interface shape.[21] Remarkably, even spherical colloids have been shown to have highly directional interactions. For example, on interfaces with constant mean curvature and weakly varying deviatoric (saddle-like) curvatures, charged spherical colloids formed a distorted square lattice due to capillary quadrupolar interactions balanced by electrostatic repulsion.[22] On interfaces with steeper deviatoric curvature gradients, isolated disk-like or spherical particles migrate to sites of high deviatoric curvature as shown in Fig.1(b), while keeping their quadrupolar rise aligned with the rise of the interface, like a charged multipole in an external electric field.[23,24] This rotation to preferred alignment is evident with isolated anisotropic particles like cylindrical microparticles; if not properly aligned when they encounter the curvature field, they rotate to align the quadrupolar axis of their distortion fields with the principal axes of the interface before migrating.[25]

These ideas, reported over the past decade, provide untapped opportunity to organize colloidal particles. In this research, we probe this organization on interfaces with zero mean curvature but varying deviatoric curvature formed around a cylindrical micropost hundreds of microns in diameter (Fig.1(a)). By considering the interactions of the overlapping distortions of the colloids on a curved interface (Fig.1(c)), we probe the formation and migration of dimers to steep curvature regions, (Fig.1(d)). For more crowded interfaces, we explore fractal structures formed around the cylindrical post by a dense suspension of microspheres (Fig.1(e)). To support these observations, we derive theory for pair interactions between colloids trapped on curved interfaces. We implement Monte Carlo simulations informed by our analysis to compare to the trapped structures formed in the regions of high curvature gradient.

2 Theory

We derive the pair interaction between two spherical particles A and B trapped on a curved fluid interface in the limit of small slopes. Particle weight and body torques are also neglected; an assumption valid in the limit of small Bond number, $Bo = \frac{\Delta\rho g a^2}{\gamma}$, where $\Delta\rho$ is the density difference between the two fluids on either side of the interface, g is the gravitational acceleration constant, a is the characteristic length of the particle, and γ is the interfacial tension. We focus here on interfaces with negligible mean curvature but finite differences in principal curvatures formed around the cylindrical micropost. For such interfaces, in the limit of small slopes, the interface shape is governed by Laplace's equation. Defining h as the height of the interface above the plane tangent to the interface, this requires $\nabla^2 h = 0$. The particles A and B have randomly pinned undulated contact lines of radius a that can be decomposed into Fourier modes with leading order modes being the quadrupole with magnitudes h_{qpA} and h_{qpB}, respectively. They are separated by distance r_{AB} and are located at a specific polar location (L_i, β_i) defined by a fixed polar coordinate centered at the cylindrical micropost of radius R_m and height H_m, as shown schematically in Fig. 2(a). The rise axis of the quadrupolar distortion made by each particle can be oriented arbitrarily on the interface with respect to the principal axes. These quadrupolar distortions vary as $\cos 2\phi$ for an angle ϕ around the particle. For isolated particles, the equilibrium orientation is for the rise axis of this distortion to be aligned along the positive principal axis of the underlying curved interface.

2.1 Method of reflections

We adopt the method of reflections to derive an analytical solution for the pair interactions between particles on curved interfaces.[26,27] In this method, the interface shape is expanded in a Taylor series in the vicinity of the particle, with terms owing to each source of disturbance, including the neighboring particle and the host interface shape. Enforcement of the pinned contact line boundary condition generates reflected modes or induced distortions in the interface.

We define a polar coordinate system (r_A, ϕ_A) with origin at the center of the circular hole of radius a made by particle A, and $\phi_A = 0$ along the x-axis. In the limit of small slopes, the shape of the host interface, i.e the interface in the absence of any particles can be locally expanded in a Taylor series around the center of A as

$$h^A_{host} = 2H^A_o \frac{r_A^2}{2} + \Delta C^A_o \frac{r_A^2}{4} \cos(2(\phi_A - \beta_A)). \quad (1)$$

In this expression, $H^A_o = \frac{1}{R^A_1} + \frac{1}{R^A_2}$ is the (negligible) mean curvature and $\Delta C^A_o = \frac{1}{R^A_1} - \frac{1}{R^A_2}$ is the deviatoric curvature evaluated at the origin of this coordinate system, where R^A_1, R^A_2 are the principal radii of curvature of the interface also evaluated at the origin of A. Thus,

$$h^A_{host} = \Delta C^A_o \frac{r_A^2}{4}\cos(2(\phi_A - \beta_A)). \tag{2}$$

The pinning of the contact line requires $h^A_p(r_A = a, \phi_A) = h_{qpA}\cos(2(\phi_A - \alpha_A))$ where α_A is the phase angle defining the orientation of the quadrupolar rise axis for particle A with respect to the polar coordinate (r_A, ϕ_A) with origin at the center of A. If A was isolated on the curved interface, the shape of the interface around the particle would be the sum of the contributions:

$$h^A_{iso}(r_A,\phi_A) = h^A_{host}(r_A,\phi_A) + h^A_p(r_A,\phi_A) + h^A_{ind,host}(r_A,\phi_A), \tag{3}$$

where $h^A_p(r_A,\phi_A) = h_{qpA}\frac{a^2}{r_A^2}\cos(2(\phi_A - \alpha_A))$ is the quadupolar distortion in the interface owing to the undulated contact line and $h^A_{ind,host}(r_A,\phi_A) = -\frac{\Delta C^A_o}{4}\frac{a^4}{r_A^2}\cos(2(\phi_A - \beta_A))$ is the reflected mode or induced mode owing to interface curvature that enforces the contact line boundary condition. Similarly a solution for the interface shape can be found near particle B expressed in a polar coordinate (r_B, ϕ_B) centered in the circular hole made in the interface by B as,

$$h^B_{iso}(r_B,\phi_B) = h^B_{host}(r_B,\phi_B) + h^B_p(r_B,\phi_B) + h^B_{ind,iso}(r_B,\phi_B). \tag{4}$$

If A and B are near each other, however, they change the shape of the interface in each other's vicinity. This change in interface shape near A by B can be found by expanding the disturbances made by particle B around the center of A in a Taylor series. Given that body forces and torques are negligible, the quadratic term in this expansion is the first to contribute. Thus, in the vicinity of A the shape of the interface due to particle B's disturbance is,

$$h_{BatA} = \frac{3h_{qpB}a^2}{r_{AB}^4} r_A^2\cos(2(\phi_A + \alpha_B)) - \frac{3\Delta C^B_o a^4}{4r_{AB}^4} {r_A}^2\cos(2(\phi_A + \beta_B)), \tag{5}$$

where the first term in the expression corresponds to the disturbance made by B in the vicinity of A on a planar interface,[14] and the second term is the correction owing to the curvature near B. We can now find the interface shape around A near B by solving the Laplace equation subject to a modified far field boundary condition which requires that

$$\lim_{r_A\to\infty} h^A(r_A,\phi_A) = h^A_{host} + h_{BatA}. \tag{6}$$

The resulting expression for h^A is the sum of contribution from (i) the quadrupolar distortion owing to A's undulated contact line, (ii) the distortion from the host interface, (iii) the local distortion near A from the neighboring particle B, (iv) the reflected mode or induced term from the distortion of the host interface, and (v) the reflected mode or induced term due to particle B.

$$h^A(r_A,\phi_A) = h^A_p + h^A_{host} + h_{BatA} + h^A_{ind,host} + h_{ind,BatA}, \tag{7}$$

where

$$h_{ind,BatA} = \\ -\frac{3h_{qpB}a^2}{{r_{AB}}^4}\frac{a^4}{{r_A}^2}\cos(2(\phi_A + \alpha_B)) + \frac{3\Delta C^B_o a^4}{4{r_{AB}}^4}\frac{a^4}{{r_A}^2}\cos(2(\phi_A + \beta_B)). \tag{8}$$

The inset in Fig.2(a) illustrates an example of the interface shape around A near B where the shape is influenced by the neighboring particle and the curvature field defined by the micropost. The quadrupolar distortion around the particle has been exaggerated for illustrative purposes. To find the pair interaction between particle A and B the excess surface area has to be calculated. In the limit of small slopes the area of the interface is approximated as $\int\left(1 + \frac{\nabla h\cdot\nabla h}{2}\right)dS$, where h is the interface shape in the presence of the particles, and dS is the area element. We first consider the free energy of the system prior to attachment of particle A, which can be written as,

$$E_1 = \gamma \oiint_D \left(1 + \frac{\nabla(h^A_{host} + h_{BatA})\cdot\nabla(h^A_{host} + h_{BatA})}{2}\right)dS, \tag{9}$$

where γ is the interfacial tension, and D refers to the entire interfacial domain. Upon attachment of particle A to the interface, the energy becomes,

$$E_2 = \gamma_1 A_1 + \gamma_2 A_2 + \gamma \oiint_{D-P}\left(1 + \frac{\nabla h^A\cdot\nabla h^A}{2}\right)dS, \tag{10}$$

where h^A is the shape of the interface after particle A is adsorbed, $\gamma_1 A_1$ and $\gamma_2 A_2$ are surface energies for the particle surface in contact with the upper and lower fluids, and $D - P$ refers to the domain of the interface outside of the particle. Calculating the change in free energy $\Delta E = E_2 - E_1$ we get,

$$\Delta E = \Delta E_{planar} - \gamma\frac{h_{qpA}a^2\Delta C^A_o}{2}\pi\cos(2(\beta_A - \alpha_A)) \\ -\gamma\frac{6h_{qpA}h_{qpB}a^4}{r_{AB}^4}\pi\cos(2(\alpha_A + \alpha_B)) + \gamma\frac{3h_{qpA}\Delta C^B_o a^6}{2r_{AB}^4}\pi\cos(2(\alpha_A + \beta_B)). \tag{11}$$

The first term is independent of curvature and accounts for the trapping energy of particle A on a planar interface, $\Delta E_{planar} = \gamma_1 A_1 + \gamma_2 A_2 + \gamma\pi h^2_{qpA} - \gamma\pi a^2$. Since the contact line is pinned, this term is a constant that we can neglect in the ensuing discussions. The second term defines the interaction between particle A and the host curvature field, E^A_{iso}. Thus, the last two terms accounts for the pair interaction between the two neighboring particles and define the pair capillary energy for particle A, E^A_{pair}. These calculations can be repeated for particle B in the vicinity of A on the curved host interface. Adding the results, gives the net curvature capillary interaction energy for a particle pair,

$$\frac{E_{net}}{\gamma\pi a^2} = E^A_{iso} + E^B_{iso} + \Bigg\{ -\frac{12 h_{qpA} h_{qpB} a^2}{r^4_{AB}} \cos(2(\alpha_A + \alpha_B)) + \frac{3 h_{qpA} \Delta C^B_o a^4}{2 r^4_{AB}} \cos(2(\alpha_A + \beta_B)) + \frac{3 h_{qpB} \Delta C^A_o a^4}{2 r^4_{AB}} \cos(2(\alpha_B + \beta_A)) \Bigg\}, \tag{12}$$

where $\Delta {C_o}^i = \frac{2R_m \tan\psi}{L_i^2}$ is the deviatoric curvature of the host interface evaluated at the location of the i-th particle, and ψ is the slope of the interface. This is the final form of the energy that captures the interaction of particles A and B with the interface curvature and with each other. If gradients in E^A_{iso} or E^B_{iso} are greater than the gradient in the dimerization term (in curly brackets), then particles move independently toward the post, else the two terms compete. The outcomes for pair assembly are complex, in that they depend on the position of the particles with respect to the micropost (L_A, L_B) and their separation distance, r_{AB}.

There are higher order modes in the interface distortion near the particle because of the undulated contact line, $h_p(r,\phi) = h_2 \frac{a^2}{r^2} \cos(2(\phi - \alpha_2)) + h_3 \frac{a^3}{r^3} \cos(3(\phi - \alpha_3)) + \ldots$ and in the expansion of the interface shape near the particle, $h_{host} = \frac{\Delta C_o}{4} r^2 \cos(2(\phi - \beta)) - \frac{1}{6} \frac{\Delta C_o}{L} r^3 \cos(3(\phi - \beta)) + \ldots$, where the subscript 2 and 3 indicate mode of deformation, i.e. the quadrupole and the hexapole, and α_n is the location of the rise axis for mode n. Higher order modes will be shown to be important in structure formation later, thus we have also derived the interaction potential for two particles A and B on the curved interface up to $n = 3$ (see SI section 1 for details). The resulting pair potential is:

$$\frac{E_{net,hex}}{\gamma\pi a^2} = \frac{E_{net}}{\gamma\pi a^2} + \frac{\Delta C^A_o}{2} \frac{a}{L_A} h_{3A} \cos 3(\beta_A - \alpha_{3A}) + \frac{\Delta C^B_o}{2} \frac{a}{L_B} h_{3B} \cos 3(\beta_B - \alpha_{3B}) + 60 \frac{a^4}{r^6_{AB}} h_{3A} h_{3B} \cos 3(\alpha_{3A} + \alpha_{3B}) + 5 \frac{a^7}{r^6_{AB}} \left[\frac{\Delta C^B_o}{L_B} h_{3A} \cos 3(\alpha_{3A} + \beta_B) + \frac{\Delta C^A_o}{L_A} h_{3B} \cos 3(\alpha_{3B} + \beta_A) \right]. \tag{13}$$

2.2 Bipolar coordinate

The exact solution to the pair interaction between two spherical particles A and B in a curved host interface as described by Equation 2 can be solved in bipolar coordinates by solving for the disturbance field created by the particles on the curved interface, $\eta = h - h_{host}$, at any point in the domain. Here h is the shape of the interface in the presence of the particles. The bipolar coordinate system has a family of spherical constant level curves consistent with the geometry of our problem, and two coordinates, $-\infty \leq \zeta \leq \infty$, and $0 \leq u \leq 2\pi$. We can relate these to Cartesian coordinates through the following transformations,

$$x = \frac{c \sinh\zeta}{\cosh\zeta - \cos u} \tag{14}$$

$$y = \frac{c \sin u}{\cosh\zeta - \cos u}, \tag{15}$$

where c is the distance from the center of the curves to the focus, and $2c$ is the distance between the two focal points. Specifically for our system c can be related to the separation distance between the two particles, r_{AB}, and the radius of the particles, a. Placing our particles along the x-axis as shown in the inset of Fig. 2(b), and stretching the circles that make up the particles to the origin in the form of an ellipse, one can relate c to known parameters as follows,

$$c^2 = \frac{1}{4}[{r_{AB}}^2 - 4a^2]. \tag{16}$$

The projection of the two particle contact line on the xy-plane correspond to contours of constant ζ namely, $\zeta = -s_A$ and $\zeta = s_B$ where

$$s_A = s_B = \cosh^{-1}\left[\frac{r_{AB}}{2a}\right]. \tag{17}$$

The disturbance field is governed by the Laplace equation which in bipolar coordinates is given by,

$$\nabla^2 \eta = \frac{(\cosh\zeta - \cos u)^2}{c^2} \left[\frac{\partial^2 h}{\partial \zeta^2} + \frac{\partial^2 h}{\partial u^2} \right] = 0. \tag{18}$$

The pinning boundary condition on the contact line requires that,

$$\eta(\zeta = -s_A) = h^A_p(r_A = a, \phi_A) - h^A_{host}(r_A = a, \phi_A) + \left[\frac{2 h_{pB} a^3}{{r_{AB}}^3} \cos(\phi_A + 2\alpha_B) - \frac{a^5 \Delta {C_o}^B}{2 {r_{AB}}^3} \cos(\phi_A + 2\beta_B) \right] \tag{19}$$

$$\eta(\zeta = s_B) = h^B_p(r_B = a, \phi_B) - h^B_{host}(r_B = a, \phi_B) + \left[\frac{a^5 \Delta {C_o}^A}{2 {r_{AB}}^3} \cos(\phi_B + 2\beta_A) - \frac{2 h_{pA} a^3}{{r_{AB}}^3} \cos(\phi_B + 2\alpha_A) \right], \tag{20}$$

where the term in the brackets is the first order term from the expansion of the i-th particle's disturbance in the vicinity of particle j. This term is subtracted because the particles have no body torque, and thus lie in the plane tangent to the interface. In the region far from the particles the interface shape must be equal to that of the host requiring that $\eta(u = 0) = \eta(u = 2\pi) = 0$. The general solution can be constructed in the form a Fourier expansion as,

$$\eta(\zeta, u) = A_0 \zeta + B_0 + \sum_{m=1}^{\infty} [C_m \cos mu + D_m \sin mu] \sinh(m(s_A + \zeta)) + [E_m \cos mu + F_m \sin mu] \sinh(m(s_B - \zeta)). \tag{21}$$

The unknowns can be found explicitly by applying boundary conditions and taking advantage of orthogonality. The net curvature capillary interaction energy is given by the product of the surface tension and the excess surface area due to the adsorption of the particles, $E_{net} = \gamma \delta A$. The excess surface area in the limit of small slopes is equal to the total surface area of the interface minus the projected surface area from the circular hole made by the particle. This can be written as,

$$\delta A = \oiint \left(1 + \frac{\nabla h \cdot \nabla h}{2}\right) dS - \oiint 1 \, dS = \oiint \frac{\nabla h \cdot \nabla h}{2} dS, \qquad (22)$$

therefore, the net curvature capillary interaction energy is,

$$E_{net} = \frac{\gamma}{2}\left[\oiint_{D-P} \nabla h \cdot \nabla h \, dS - \oiint_{D-P_A} \nabla h_p^A \cdot \nabla h_p^A \, dS - \oiint_{D-P_B} \nabla h_p^B \cdot \nabla h_p^B \, dS \right], \qquad (23)$$

where the first integral is the total excess surface area around the interacting particles and host interface, and the last two are the areas around the isolated particles due to particles' self distortion. The total excess area has information about the self energies of individual particles, therefore the integrals describing these interactions have to be removed from the total energy to capture solely the interaction between the particles and the host interface. Note that $h = \eta + h_{host}$ thus the solution to the shape of the interface can be constructed and the energy can be numerically integrated.

Considering an ideal case in which particles are aligned with each other and the curvature field, i.e. $\alpha_A = \beta_A, \alpha_A = \alpha_B$ and $\alpha_B = \beta_B$ in Equation 12, the analytical solution can be compared to the exact solution in bipolar coordinates. Fig. 2(b) shows a plot of the non-dimensional pair interaction energy as a function of the non-dimensional inter-particle distance. Both solutions display energy minimization showing that the energy should decrease as these particles come into contact. The two solutions are in agreement when the particles are far from each other as expected, but near contact, the exact solution deviates slightly from the analytical solution. This indicates that higher order reflections, which are neglected in the method of reflections, become important near field.

3 Experiments

We study the pair assembly and structure formation of polystyrene colloidal spheres (Polysciences Inc.) with mean diameter of $2a = 10\ \mu m$. These particles have been previously characterized by SEM and AFM measurements and reported to have root mean squared roughness of 15–40 *nm*. From prior work on isolated spheres on curved interfaces, it was inferred from particle trajectories that these particles have quadrupolar distortions with magnitudes ranging from 15–130 *nm*.[24]

The vessel in which we form the curved fluid interface is described in detail in reference [23-24], and described briefly here. A circular ring 25 μm high and several capillary lengths in radius is formed on a silicon wafer support. Centered in this ring, a circular micropost 200 μm high with radius $R_m \sim 125\ \mu m$ is fabricated. The ring and micropost are formed from SU-8 epoxy resin using standard lithographic techniques. The host curved interface is formed by pinning the interface of a drop of water to the edge of the micropost; the water is confined by the ring-like barrier. The volume of fluid is adjusted to form an interface with a small slope, $\psi \sim 5$–15^o at the three phase contact line where the micropost and interface meet. In the vicinity of the micropost, the interface has a well-defined curvature field, with negligible mean curvature due to the finite volume of fluid creating a weak but negligible pressure drop across the interface, and finite deviatoric curvature that depends on the distance from the center of the micropost. A layer of hexadecane is gently placed on the water to prevent evaporation, and to minimize disturbance from uncontrolled convection in the laboratory. The oil superphase also facilitates introduction of particles to the interface; particles are introduced from a drop of microspheres in hexadecane added on top of the oil phase. These particles sediment and attach to the interface. Once attached to the interface, particles migrate uphill along deviatoric curvature gradients, form pair assemblies with neighboring particles, and assemble into structures whose packings we characterize and compare to simulations.

4 Monte Carlo simulations

To study multiparticle assemblies, we perform Monte Carlo (MC) simulations to explore the energy landscape of our system and to extract structural data. In the model system, both the colloids and the micropost are represented as hard spheres with radius a and $25a$ respectively, and all pair interactions were calculated using Equation 12. We initialize a system of N colloidal particles by assigning a random position to each colloid around the micropost within a circle of radius R_{range}. For each particle i, the quadrupolar rise is included by defining an in-plane unit vector $\hat{n}_i$ with a π rotational symmetry. The rise directions are also chosen to be random in the initial configuration. The system evolves through a set of three MC moves namely (i) translation, (ii) rotation and (iii) cluster move.

In the translational move, the centre of a randomly chosen colloidal particle, X_c, is moved to a new random position $X_c + \delta X$ within a cube of size ε centered at X_c. In the rotational MC move, a colloidal particle is chosen randomly and the rise orientation $\hat{n}_i$ for the chosen colloid is rotated by a randomly chosen angle $\delta\theta$ drawn from a uniform distribution in the range $[-\pi/200, \pi/200]$. Both the rotational and translational moves are accepted through standard Metropolis algorithm,[28] according to the probability $\min(1, \exp(-\beta\Delta U))$ where ΔU is the change in total energy upon change in the degree of freedom. For all the MC moves the energetics is controlled by the total energy of the system of colloids $U = \sum_i E_{i,p}^{HS} + \sum_{\langle i,j \rangle} E_{i,j} + E_{i,j}^{HS}$, where the first summation is over all the colloids and the second is over all the pairs. Here $E_{i,j}$ is the net curvature capillary interaction energy of the colloids at the interface given in Equation 12 while $E_{i,j}^{HS}$, $E_{i,p}^{HS}$ are hard sphere potentials representing colloid-colloid and colloid-micropost excluded volume interactions respectively. To perform a cluster move, we first find the clusters of colloids by defining a cutoff distance r_{cut} for two particles to form a cluster. In a cluster move, a randomly selected cluster is attempted to translate without changing the quadrupolar rise orientations of the particles within the cluster, i.e., the centre of all the particles in the selected cluster $\{\mathbf{X}_c^i\}$ is moved to a new position $\{\mathbf{X}_c^i + \delta\mathbf{X}_{cluster}\}$. The moves are accepted with an acceptance probability $\min\left\{1, \exp(-\beta\Delta U)\prod_{k,l}\frac{1-p^n(k,l)}{1-p^o(k,l)}\right\}$ where ΔU is the change in total energy upon change in positions. $p(k,l)$ is the probability of particles k and l to be in the same cluster where k

denotes a particle in the cluster and l a particle outside it. 'o' and 'n' corresponds to the old and new configurations. The acceptance rule guarantees that two particles that did not belong to the same cluster in the old configuration will not end up in a distance less than r_{cut}.[29,30] Each MC step consists of N attempted translational and rotational moves and $N_{cluster}$ cluster moves where $N_{cluster}$ is the total number of clusters. A typical colloidal aggregation run takes 5×10^5 MC steps to aggregate and a real time of 11 hours on an 8 CPU node with OPENMP parallelization. For few sample configurations we performed simulations up to 2×10^6 MC steps and observed statistically similar conformational properties.

To account for hexapolar interactions in MC we define an additional vector $\hat{n}_i^h$ in our MC simulations, with a $2\pi/3$ rotational symmetry, that is representative of the hexapolar rise at each colloidal particle i. $\hat{n}_i^h$ for each colloid is initialized randomly and is independent of the quadrupolar rise directions. In this case the rotational MC move also includes the rotation of the hexapolar orientation with the same angular displacement as used for the quadrupolar rise. For this system all energy calculations were done using the net curvature capillary interaction energy $E_{i,j}$ given in Equation 13.

5 Results and discussion

We have observed pairs of spherical particles interacting in the curvature field around the micropost upon the addition of particles to the interface. To study the dynamics of pair formation in experiment, we select pairs that are one behind the other; we inferred that the quadrupolar rise axes are aligned with the principal axes of the interface, allowing us to simplify the analysis considerably. Fig.2(c-d) shows the trajectory for two particles interacting on the curved interface. This interaction shows two particles located in a region close to the micropost, and separated by some inter-particle distance. Initially, the particles are well separated and migrate along a radial path, i.e. along deviatoric curvature gradients in the host interface, toward the micropost. When the particles are close enough to interact, particle A (pink) reverses its direction to form a dimer with particle B (green) as shown in the time stamped image (Fig.2(c)). The observation that both particles are migrating along the radial path suggests that their quadrupolar rise axes are aligned along the rise axis of the host interface via interaction with the underlying curvature field.

The dynamics of this two-particle system can also be explored. Given the deterministic particle motion evident in the experiment, stochastic forces on the particle can be neglected. The particle moves in a viscous medium with velocity u in creeping flow; the corresponding Reynolds number, $Re=\frac{au\rho}{\mu}\sim10^{-6}$, where ρ is the average fluid density and μ is the average viscosity of the superphase and subphase. In this limit, capillary forces are balanced by viscous drag for each particle. Equating the capillary force $F_{cap}=-\nabla E_{net}$ to the Stoke's drag force $F_{drag}=6\pi\mu a\frac{dL}{dt}$, assuming a constant drag coefficient, and using our analysis (Equation 12), we can predict the change in particle position with respect to the post over time. Fig.2(d) shows a plot of the distance from the particle center to the post as a function of time for particle A and B. The comparison between the predicted behavior and the observed trajectory shows that there is good agreement between the solutions in the far field. However, near field there is a slight deviation between the two, attributable to near field interactions or to the constant drag coefficient assumption. By integration of energy dissipated along the particle path, the change in the net curvature capillary interaction energy between the particles is inferred to be order 10^4k_BT, and forces are of order 10^{-1} pN. The magnitude of the quadrupolar distortions are the sole free parameters fit in this comparison. Their magnitude ($h_{qpA}=15\ nm$, $h_{qpB}=36\ nm$) is similar to those previously inferred for spherical polystyrene particles moving in isolation on curved interfaces; those magnitudes differed from particle to particle. This analysis indicates that capillary forces and torques from curvature drive particles to sites of high curvature and alignment of quadrupolar axes along principal axes; those from neighboring particles drive mirror symmetric orientations and assembly, and the reflected modes from the curvature favor yet a third orientation when minimizing the interfacial area created by the particle. Analysis for other set of interacting pairs can be found in SI, section 2.

5.1 Dimer formation

The specific trajectory described above is one of multiple trajectories observed experimentally for particles on the curved interface. For other particle pairs, dimers can form with different orientations of their line of centers aligned along neither principal axis, or can fail to form entirely, depending on their position with respect to the post and each other, and the orientation of their quadrupolar axes. We know that when deviatoric curvature is very weak (large distances from the post) the term in curly brackets in Equation 12 will dominate and particles will dimerize. On the other hand, cases in which particles are well-separated the curvature field always dominate. In this case particles migrate to sites of high curvature in isolation. In all other cases, the curvature and pair interactions compete with a wide variety of possible assemblies. Compared to isolated particles which are known to follow a radial path along curvature gradients (See SI section 3 for details) and align their quadrupolar rise axis along the rise axis of the host interface, pairs have the freedom to depart from these paths. Fig.3(a) shows a few examples of dimerization events. The first panel shows assembly in which particles are right behind one another, both following a radial path to the edge of the micropost and forming a pair along the way. The assemblies pictured in panels II and III are examples of particles moving along complex paths to make dimers with lines of centers that do not align along either principal axis. These observations show that there is an interplay between the interface curvature, the particle separation distance, and the particle orientation. Furthermore, in the near field, other modes of distortion in the interface from the undulated contact line can play a role. (We develop this concept in greater detail below).

Consider the net capillary energy for particle i in the vicinity of particle j. Expressing deviatoric curvature in terms of the coordinates of the interface and factoring out the isolated particle curvature migration term,

$$\frac{E^i_{net}}{\gamma\pi a^2} = -R_m \tan\psi \frac{h_{qpi}}{L_i^2}\cos(2(\beta_i-\alpha_i))\times$$

$$\left[1+\left\{\frac{6h_{qpj}}{R_m\tan\psi}\frac{L_i^2 a^2}{r_{AB}^4}\frac{\cos(2(\alpha_i+\alpha_j))}{\cos(2(\beta_i-\alpha_i))} - \frac{L_i^2}{L_j^2}\frac{3a^4}{r_{AB}^4}\frac{\cos(2(\alpha_i+\beta_j))}{\cos(2(\beta_i-\alpha_i))}\right\}\right]. \tag{24}$$

For pair interaction to dominate the terms inside the curly bracket must be greater than one. These terms depend in a complex manner on quadrupolar rise axis alignment with respect to the post and between neighbors. The torques that enforce these alignments, given by angular derivatives of Equation 24, decay more slowly than do capillary forces. Evaluation of this expression for typical system parameters specified in the caption to Fig.3, shows that the first term in curly brackets is typically one order of magnitude greater than the second term. Furthermore, the ratio $\frac{6h_{qp}}{R_m\tan\psi}$ is $\sim 10^{-2}$, so pair interactions are important only when:

$$\tilde{L_i} \gg \tilde{r_{AB}}^2, \tag{25}$$

where $\tilde{L_i}$ and $\tilde{r_{AB}}$ are the distances normalized by particle radius. For this particular arrangement, the third term is relatively small. However, more generally, all three terms can compete. While the net capillary energy depends on particle location, alignment, and particle orientation with respect to one another, we can enumerate several expected assemblies. These have been captured by MC simulations for particles with constant quadrupolar magnitudes shown in Fig.3(b). Initially the particles are placed side by side and the rise orientations are taken to be in random directions. The distance from the post center to the particle center for A, L_A, was 350 μm for all simulations, and the initial separation distance between the particles was gradually increased.

I. Pair assembly with no curvature alignment. When the magnitude of the torque due to particle-curvature interaction is small compared to the torque resulting from particle-particle interactions, particles dimerize in a mirror symmetric state without influence from the underlying curvature field. As shown in panel I of Fig.3(b) this occurs only for particles at close distances. This assembly will happen with greater probability on interfaces that are crowded since particles tend to land close to one another.

II. Pair assembly with weak migration. If the magnitude of the deviatoric curvature generated torque is large enough to drive alignment along principal axes, particles can dimerize along the azimuthal direction (panel II of Fig.3(b)) or the radial direction (not shown). Particles align with the curvature field and each other, and then come together to form a dimer, $\cos(2(\alpha_A+\alpha_B)) \approx \cos(2(\beta_i-\alpha_i))$. Here, particles form dimers with minimal migration to sites of high deviatoric curvature.

III. Pair assembly with migration. Similar to the case described above, if particles are at regions of strong curvature they will first align with the curvature field. However, as they are well-separated, initially the curvature dominates their interaction. Particles migrate in isolation until close enough to form a pair (Fig.2(c-d) and panel III of Fig.3(b)). Otherwise, if the particles are far apart, particles will fail to form a pair (IV of Fig.3(b)).

5.2 Structure formation

In experiment we have also characterized structures formed by a dense suspension of 5-micron radius polystyrene spheres at the hexadecane-water curved interface formed around a 125-micron radius cylindrical post, as shown earlier in Fig.1(e). Close to the post the fractal structure shows curvature-dominated linear structures. At large L, the structures are more highly branched. These branched structures are formed by particle clusters that formed along the path to the post. Fig.4(a) shows close ups of clusters of particles showing complex configurations including linear and square structures (straight chains and L shape). We also observe hexagonal assemblies (triangles, Y shapes), and other complex formations that arise from the overlapping of smaller groups. Just like isolated particles these migrate toward regions of high curvature and once attached become hot spots for other groups and particles. We see both isolated particles migrate to the post and join the tips of the closest structure, and aggregates joining to form the branched structure. Once a particle joins a cluster, it does not leave it. However, there is significant reorganization within a cluster as it migrates due to the change in balance of the curvature-related interactions, including changes in relative particle position and rotation of particles. Thus, these structures are not strictly kinetically trapped. Example of a cluster reorganizing in experiment is shown in the supplementary video S9 (e.g. a particle within an L shape changes position in the cluster).

The observed linear and square assemblies are purely from quadrupolar interactions. On the other hand the more complex structures were suspected to come from near field interactions due to higher order modes in the interface distortion near the particle, and in the expansion of the interface shape near the particle. These higher order terms drive other symmetries for pair interactions and for alignment and migration in the host interface curvature field. These factors also affect the clusters. To predict some of these assemblies we derived the pair potential including the next mode for the particle's self-distortion and interface shape, the hexapole. This potential given in Equation 13 was then implemented in MC simulations. Fig.4(b) shows the assemblies obtained from a 200-particle MC simulation. As in experiments, the simulation captures close packed triangle, hexagonal caps, and other assemblies where chains are slightly bent. Square and complex assemblies are also present.

The distribution of angles calculated from each particle center in the particle aggregates yields evidence of different mechanisms behind the formation of these structures. Fig.5(a) and Fig.5(b) show the angle distribution between particle centers for fractals created by capillary interactions on interfaces with $\psi = 5^o$ and $\psi = 15^o$ respectively. Each angle distribution has distinct peaks at $60^o, 90^o$ and 180^o. The peaks at 90^o, and 180^o suggest the presence of quadrupolar interactions on the curved interface. The peak at 60^o shows the importance of higher orders modes in the formation of structures. These peaks are absent in a simulated DLA structure with a circular seed region (i.e. the post) and the same number of particles ($\sim$ 664) as in one of the experiments (Fig. S6(d)). We have also simulated systems of 500 particles where hexapolar interactions are included and where we have assumed the magnitude of the hexapolar distortion is equal to that of the quadrupole ($h_{qp} = 30\ nm = h_{hex}$).

When comparing the angle distribution in the clusters between experiments and MC simulations, very clear peaks appear in the simulations for $60^o, 90^o$ and 180^o, which are blurred in the experiments. These differences cannot be attributed to MC displacements or rotational step sizes (See SI section $S6$ for details). However, two key differences in theory/simulation and experiment likely explain this discrepancy. Namely, the pair potentials on which the simulations rely do not include the higher order modes in the particle disturbances, and assume fixed amplitudes of the quadrupolar and hexapolar modes. However, this confirms that these interactions are present and are important in capturing structure formation on the curved interface. Recall that these structures include particles that form clusters far from the post. On interfaces with steeper slopes, we observed faster clustering, owing to the increased importance of the third term in Equation 24 (Fig.5(d)). The success of MC in capturing these effects relies on the cluster moves. The fact that MC simulations capture aspects of the particle assemblies and trajectories may reflect that hydrodynamic interactions play a secondary role. However, drag on particles and hydrodynamic interactions for particles in close proximity at fluid interfaces is a complex topic and worthy of detailed future study.

The overall fractal structures have fractal dimension ranging from 1.4–1.6, which is the same as that of the commonly known diffusive limited aggregation (DLA) [31] fractal structure in the limit of small particle number (see SI section 5 for details). The fractal dimension of the capillary structures depends only weakly on the number of particles N, as shown in Fig.5(e). In this figure, the asterisks correspond to the DLA limit for 567, 664 and 6000 particles. In experiment, we have formed two structures, with 567 and 664 particles, respectively; the fractal dimensions of these structures, shown as triangles, are 1.46 and 1.52, respectively. To further explore the dependence on N, we use MC simulations to compute the fractal dimension for simulated capillary assemblies for 500, 750, 1000, and 1500 particles. For each value, five runs with different particle positions and quadrupole orientations were performed and the standard deviation was calculated, showing we obtain similar metrics ($SD = 0.01$–0.04). Corresponding structures for realizations of the MC simulations ($N = 1000$) and the DLA ($N = 1000$) are shown in Fig.5(e).

6 Conclusion

We study colloidal organization at curved fluid interfaces owing to particle-curvature and particle-particle capillary interactions in theory, simulations, and experiment. We show that we are able to derive the pair capillary energy for two particles on a curved fluid interface with varying deviatoric curvature using the method of reflections. The exact solution can also be derived in bipolar coordinates in the form of a series, which can be evaluated and compared to the solution using method of reflections. Both solutions agree well in the far field as expected. In the near field, however, the solutions differ since the exact solution captures near field distortions neglected in the more approximate method, which yields a closed form solution. This comparison shows that the analytical solution is a good approximation except very near contact, and gives good insight about the physics of the problem.

The interaction potential can also be used to predict assembly of particle pairs through Monte Carlo simulations, and dynamics through force calculations. The predicted particle behavior agrees with observed experimental trajectories. The data allows the particle quadrupolar magnitudes to be inferred. The cases explored showed that the magnitudes are consistent to magnitudes previously reported and comparable to particle roughness. Group assemblies and fractal like structures around the cylindrical micropost have been observed experimentally. Monte Carlo simulations indicated that the assemblies seen are due to the coupling of quadrupolar interactions in the far field but also due to near field interactions from higher order modes. Angle distributions between particle centers yield evidence that these structures are formed due to unique interactions that arise from the coupling of particle deformation and the curvature field underneath them.

Conflicts of interest

There are no conflicts to declare.

Acknowledgements

Discussions with Drs. Nima Sharifi Mood and Nicholas Chisholm are gratefully acknowledged. This work is partially supported by NSF grants CBET-1133267, CBET-1066284, GAANN P200A120246, MRSEC grant DMR11-20901, and NIH grant U54CA193417.

Notes and references

1 R. G. Willaert and G. V. Baron, *Reviews in Chemical Engineering*, 1996, **12**, 1–205.

2 T. Jesionowski, *Colloids and Surfaces A: Physicochemical and Engineering Aspects*, 2001, **190**, 153–165.

3 Y. Zhai, Y. Ma, S. N. David, D. Zhao, R. Lou, G. Tan, R. Yang and X. Yin, *Science*, 2017, **355**, 1062–1066.

4 D. Baranov, A. Fiore, M. van Huis, C. Giannini, A. Falqui, U. Lafont, H. Zandbergen, M. Zanella, R. Cingolani and L. Manna, *Nano Letters*, 2010, **10**, 743–749.

5 S. L. Biswal and A. P. Gast, *Physical Review E*, 2003, **68**, 021402.

6 S. L. Biswal and A. P. Gast, *Physical Review E*, 2004, **69**, 041406.

7 P. Dommersnes, Z. Rozynek, A. Mikkelsen, R. Castberg, K. Kjerstad, K. Hersvik and J. O. Fossum, *Nature Communications*, 2013, **4**, 2066.

8 A. Dong, J. Chen, P. M. Vora, J. M. Kikkawa and C. B. Murray, *Nature*, 2010, **466**, 474–477.

9 P. Pieranski, *Physical Review Letters*, 1980, **45**, 569.

10 B. J. Park and D. Lee, *Small*, 2015, **11**, 4560–4567.

11 G. Meng, J. Paulose, D. R. Nelson and V. N. Manoharan, *Science*, 2014, **343**, 634–637.

12 W. T. Irvine, V. Vitelli and P. M. Chaikin, *Nature*, 2010, **468**, 947–951.

13 I. B. Liu, N. Sharifi-Mood and K. J. Stebe, *Annual Review of Condensed Matter Physics*, 2018, **9**, 283–305.

14 D. Stamou, C. Duschl and D. Johannsmann, *Physical Review E*, 2000, **62**, 5263.

15 P. A. Kralchevsky and K. Nagayama, *Advances in Colloid and Interface Science*, 2000, **85**, 145–192.

16 M. Oettel, A. Dominguez and S. Dietrich, *Physical Review E*, 2005, **71**, 051401.

17 D. M. Kaz, R. McGorty, M. Mani, M. P. Brenner and V. N. Manoharan, *Nature Materials*, 2012, **11**, 138–142.

18 J.-C. Loudet, A. M. Alsayed, J. Zhang and A. G. Yodh, *Physical Review Letters*, 2005, **94**, 018301.

19 L. Botto, L. Yao, R. Leheny and K. Stebe, *Soft Matter*, 2012, **8**, 4971–4979.

20 V. Paunov, P. Kralchevsky, N. Denkov and K. Nagayama, *Journal of Colloid and Interface Science*, 1993, **157**, 100–112.

21 E. Lewandowski, J. Bernate, P. Searson and K. Stebe, *Langmuir*, 2008, **24**, 9302–9307.

22 D. Ershov, J. Sprakel, J. Appel, M. A. C. Stuart and J. van der Gucht, *Proceedings of the National Academy of Sciences*, 2013, **110**, 9220–9224.

23 L. Yao, N. Sharifi-Mood, I. B. Liu and K. J. Stebe, *Journal of Colloid and Interface Science*, 2015, **449**, 436–442.

24 N. Sharifi-Mood, I. B. Liu and K. J. Stebe, *Soft Matter*, 2015, **11**, 6768–6779.

25 M. Cavallaro, L. Botto, E. P. Lewandowski, M. Wang and K. J. Stebe, *Proceedings of the National Academy of Sciences*, 2011, **108**, 20923–20928.

26 J. Happel and H. Brenner, *Low Reynolds number hydrodynamics: with special applications to particulate media*, Springer Science & Business Media, 2012, vol. 1.

27 S. Kim and S. J. Karrila, *Microhydrodynamics: principles and selected applications*, Courier Corporation, 2013.

28 N. Metropolis, A. W. Rosenbluth, M. N. Rosenbluth, A. H. Teller and E. Teller, *The Journal of Chemical Physics*, 1953, **21**, 1087–1092.

29 D. Wu, D. Chandler and B. Smit, *The Journal of Physical Chemistry*, 1992, **96**, 4077–4083.

30 D. Frenkel and B. Smit, *Understanding molecular simulation: from algorithms to applications*, Elsevier, 2001, vol. 1.

31 T. A. Witten and L. M. Sander, *Physical Review B*, 1983, **27**, 5686.

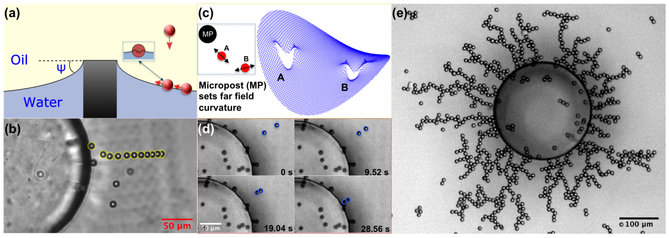

Fig. 1 (a) Schematic representation of two spherical colloids (red spheres) on a curved interface formed by a cylindrical micropost (black rectangle). *Inset*: schematic representation of a sphere with a pinned undulated contact line. (b) Time lapsed image of the migration of an isolated $10\ \mu m$ PS sphere on the curved interface. The trajectory is shown in yellow for equal time steps of $3.26\ s$ (the neighboring colloids are sedimenting in the oil phase and are not yet adsorbed in the interface). (c) Distortions from particles A and B on the curved interface are depicted with random orientation of the quadrupolar rise axis with respect to each other and the principal axis of the underlying curvature. The curved fluid interface has a saddle shape in the vicinity of the particles defined by the neighboring particle and the curvature field defined by the micropost. *Inset*: top view of the two spherical colloids (red circles) on the curved interface formed by the cylindrical micropost (black circle). Arrows indicate location of the quadrupolar rise axes. (d) Time stamped images of two particles shown in blue interacting and forming a dimer on the curved interface. (e) Fractal structure around the cylindrical micropost formed from migrating groups and isolated particles on the curved interface with slope $\psi = 5^o$. Particles on top of the micropost are not in the fluid interface and are not considered as part of the structure. The fractal dimension of the structure is $D = 1.52$.

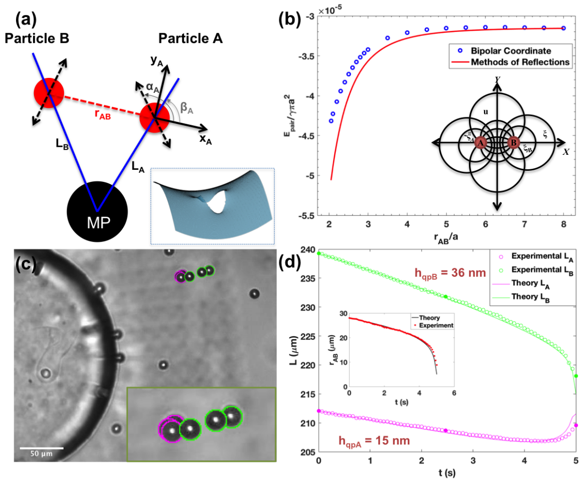

Fig. 2 (a) Top view of two spherical colloids (red circles) on a curved interface formed by a cylindrical micropost (black circle). *Inset:* distortion from particle A on the curved interface. (b) Dimensionless pair interaction energy obtained from method of reflections (solid line) and exact solution obtained from analysis in bipolar coordinate (open circles) as a function of the dimensionless inter-particle distance. *Inset*: sketch of the bipolar coordinates system in the x-y plane with the line that connects the centers of the two particles on the x axis (red circles). (c) Time stamped image of two particles migrating toward the post and forming a dimer $(t = 0s, t = 2.47s, t = 5s)$. *Inset*: close-up of the trajectory (d) The trajectory of each particles in this dimer (symbols) in terms of position with respect to the micropost L versus time t. Theory with best fit amplitudes for quadrupolar distortions (solid lines). *Inset*: inter-particle distance r_{AB} versus time t.

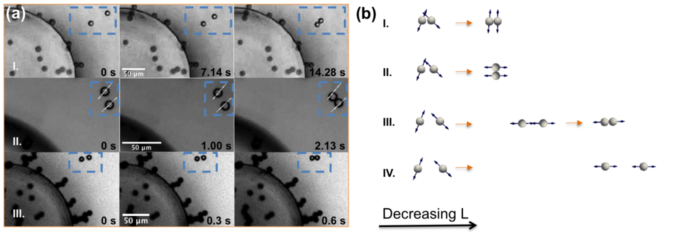

Fig. 3 Particle dimerization at the curved interface: (a) Experimental observations of two particles interacting on the curved interface showing different behaviors. (I) Particles form dimer along the radial direction with respect to the micropost, indicating quadroples aligned along curvature rise axis. (II-III) Particles can form dimers oriented at different angles with respect to the radial direction, indicating importance of the other terms in Equation 24. (b) Monte Carlo simulation using interaction potential derived for two particles on a curved interface showing different expected behaviors at $L_A = 350\ \mu m$ for a typical system with $\psi = 15^o$, $a = 5\ \mu m$, $R_m = 125\ \mu m$, and $h_{qpA} = h_{qpB} = 30\ nm$. Particles are initially side by side with a random orientation of their quadrupolar axes. (I) Particles can dimerize without influence from the underlying curvature field. (II) Particles align with the curvature and form dimer along the azimuthal direction. (III) Particles align with the curvature field, migrate some distance and then assemble. (IV) Particles migrate in isolation.

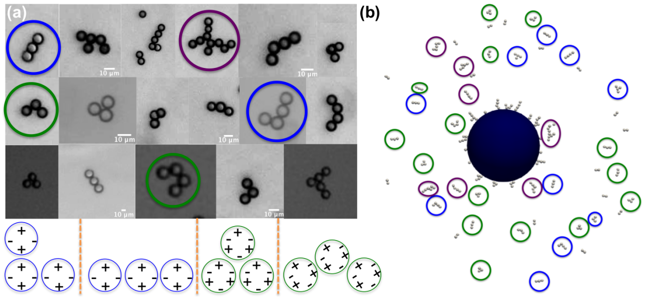

Fig. 4 Structure formation at the curved interface: (a) Multi-particle groups formed in experiment on the curved fluid interface for slopes ψ between 5^o and 15^o. Diagram below correspond to some of the observed shapes labelled with $+$ and $-$ signs to correspond to regions of quadrupolar rise and quadrupolar fall respectively. (b) Monte Carlo simulation of groups formed from quadrupolar and higher order hexapolar interactions using derived modified pair potential for a typical system with $\psi = 15^o$, $a = 5\ \mu m$, $R_m = 125\ \mu m$, and $h_{qpA} = h_{qpB} = 30\ nm$. Snapshot is at the 69,000 MC step. [Blue circles] linear and square assemblies (right angles), [Green circles] hexagonal assemblies, [Purple] complex assemblies.

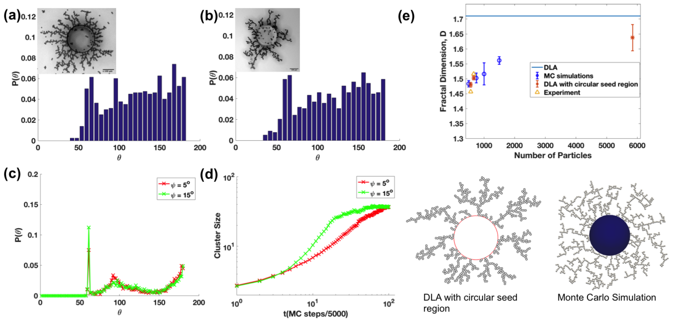

Fig. 5 Angle distribution between particle centers for fractal structure observed in experiments (shown in inset) when (a) $\psi = 5^o$ $(D = 1.52)$ and (b) $\psi = 15^o$ $(D = 1.46)$. (c) Angle distribution for simulated fractal of 500 particles using MC with higher order hexapolar distortions. (d) Average cluster size over MC steps. (e) Fractal dimension D versus number of particles N for fractals obtained through experiment, MC simulations, and DLA simulations. Pictures below correspond to a simulated DLA fractal with a circular seed region, and to a MC simulated fractal with 664 and 1000 particles respectively.

Graphical and textual abstract

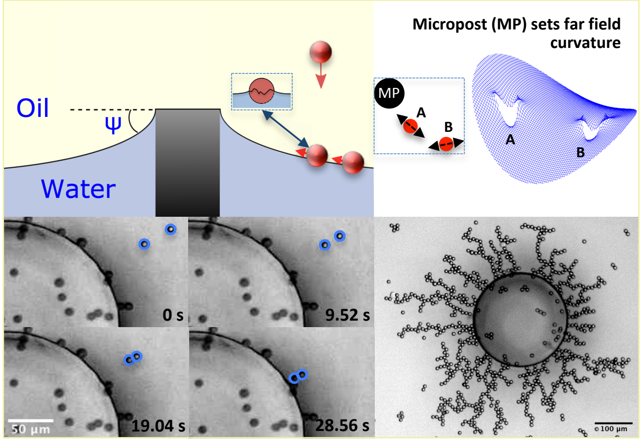

We probe colloidal organization by considering the interactions of the overlapping distortions of colloids on a curved interface.